Thermodynamic analysis of brine management methods: Zero-discharge desalination and salinity-gradient power production

Citation: Chung, Hyung Won, Kishor G. Nayar, Jaichander Swaminathan, Karim M. Chehayeb, and John H. Lienhard V. "Thermodynamic Analysis of Brine Management Methods: Zero-Discharge Desalination and Salinity-Gradient Power Production." Desalination 404 (February 2017): 291–303.

As Published: http://dx.doi.org/10.1016/j.desal.2016.11.022

Publisher: Elsevier B.V.

Persistent URL: http://hdl.handle.net/1721.1/107713

Version: Author's final manuscript: final author's manuscript post peer review, without publisher's formatting or copy editing

Thermodynamic analysis of brine management methods: zero-discharge desalination and salinity-gradient power production

Hyung Won Chung, Kishor G. Nayar, Jaichander Swaminathan, Karim M. Chehayeb, John H. Lienhard V*

Rohsenow Kendall Heat Transfer Laboratory, Department of Mechanical Engineering, Massachusetts Institute of Technology, Cambridge MA 02139-4307 USA

Abstract

Growing desalination capacity worldwide has made management of discharge brines an increasingly urgent environmental challenge. An important step in understanding how to choose between different brine management processes is to study the energetics of these processes. In this paper, we analyze two different ways of managing highly saline brines. The first method is complete separation with production of salts (i.e., zero-discharge desalination or ZDD). Thermodynamic limits of the ZDD process were calculated. This result was applied to the state-of-the-art industrial ZDD process to quantify how close these systems are to the thermodynamic limit, and to compare the energy consumption of the brine concentration step to the crystallization step. We conclude that the brine concentration step has more potential for improvement compared to the crystallization step. The second brine management method considered is salinity-gradient power generation through pressure-retarded osmosis (PRO), which utilizes the brine's high concentration to produce useful work while reducing its concentration by mixing the brine with a lower salinity stream in a controlled manner. We model the PRO system coupled with a desalination system using a detailed numerical optimization, which resulted in about 0.42 kWh/m^3 of energy saving.

Keywords: Brine management; Zero-discharge desalination; Zero-liquid discharge; ZLD; PRO; Salt production

H.W. Chung, K.G. Nayar, J. Swaminathan, K.M. Chehayeb, and J.H. Lienhard V, "Thermodynamic analysis of brine management methods: zero-discharge desalination and salinity-gradient power production," *Desalination*, 404:291-303, 17 Feb. 2017.

*Corresponding author: lienhard@mit.edu

Nomenclature

Roman Symbols

a	Activity
A	Membrane permeability, L/m^2-hr-bar
A_m	Membrane area, m^2
B	Solute permeability coefficient, L/m^2-hr
D	Diffusion coefficient, m^2/s
E	Energy transfer per volume, kWh/m^3
f	Friction factor
g	specific Gibbs energy, J/kg-K
$\bar{g}$	partial molar Gibbs energy, J/mol-K
J	Flux, L/m^2-hr
k	Mass transfer coefficient, m/s
M	Molar mass, g/mol
MR	mass flow rate recovery ratio of draw and feed streams
$\dot{m}$	Mass flow rate, kg/s
$\dot{N}$	Molar flow rate, mol/s
q	Specific heat transfer, kJ/kg
$\dot{Q}$	Heat transfer, kW
P	Pressure, bar
Re	Reynolds number
RR	recovery ratio
s	Salinity, g/kg
S	Structural parameter, µm
Sc	Schmidt number
Sh	Sherwood number
T	Temperature, °C
v	Velocity, m/s
$\dot{W}$	Work transfer, kW
w	Specific work transfer, kJ/kg

Greek Symbols

η_{II}	Second Law efficiency
η_{comp}	Compressor efficiency
$\dot{\Xi}$	Exergy flow rate, kW
Π	Osmotic pressure, bar
ΔT_{TTD}	Terminal temperature difference, K

Subscripts

0	Ambient state
bc	Brine concentration
crys	Crystallization
b	Brine stream
d	Draw stream
desal	Desalination
power	Power production
f	Feed stream
H	Heat source
p	Pure water
in	Energy input to the system
m	Membrane surface
net	Net osmotic driving force (osmotic pressure − hydraulic pressure)
out	Energy output of the system
s	Salt
sat	Saturation
sw	Seawater stream

Superscripts

least	Thermodynamic least work of separation
max	Thermodynamic maximum work of mixing
MVC	Mechanical Vapor Compression system
rev	Reversible system
sat	Saturated state

1. Introduction

Desalination produces a concentrated brine which has to be discharged back to the environment. Brine management has become a challenging task due to large increases in desalination capacity. In 2015, global desalination capacity reached 87 Mm^3/day, of which 51 Mm^3/day is seawater desalination. Figure 1 shows the growth of the global desalination capacity over recent years [1–6].

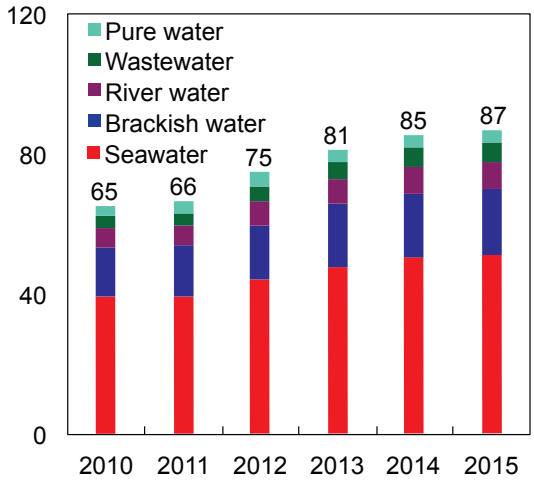

Figure 1: Global desalination capacity based on the feed water type.

Seawater desalination has a recovery of roughly 50% [7], producing nearly equal flows of brine and product. Recovery varies greatly for the desalination of different feed waters, which makes it hard to estimate the volume of brine discharge knowing only the treated water production rate. As a conservative estimate, over 50 Mm^3 of brine is discharged everyday. This large and growing quantity of brine should be managed with care in order to avoid harmful environmental effects.

One method of mitigating the environmental concerns from brine discharge is by avoiding discharge all together through the usage of zero-discharge desalination (ZDD) designs, which should be differentiated from zero-liquid discharge (ZLD) because ZDD does not even discharge salt. Near-ZDD designs have been implemented commercially for producing salt from seawater [8, 9]. Economically feasible ZDD system designs for seawater desalination have also been proposed [10]. ZDD and ZLD systems broadly use two steps/sub-systems: a brine concentration step that concentrates the feed stream to near saturation conditions, and a crystallization step where saturated brine is completely crystallized. Several technology options exist for the brine concentration and crystallization steps. For the brine concentration step, the technologies that have been deployed industrially include: electrodialysis (ED) [8, 9], mechanical vapor compression systems (MVC) [11–13], and solar evaporation ponds [11, 14]. In Japan, electrodialysis (ED) has been used extensively for concentrating brine for salt production [8]. In such systems, incoming seawater feed is split into diluate

and concentrate streams. The feed in the concentrate stream is typically concentrated from 35 g/kg to 200 g/kg while the diluate is diluted to slightly less than 35 g/kg and discharged back into the sea. ED systems are appropriate when partial desalination is an option [15]. For complete brine concentration producing pure product water, MVC systems are primarily used. The crystallization step in ZDD and ZLD is typically achieved through multi-effect evaporators [11] or solar evaporation ponds [11, 14]. Apart from the above processes, newer processes such as SAL-PROC also exist where brine is sequentially crystallized using both evaporation and chemical processing [16]. More recently, membrane distillation (MD) has emerged as an alternative technology for an integrated brine concentration and crystallization process due to its ability to handle highly concentrated feed water [17–21].

Another method of handling brine discharge is to utilize the brine's exergy to produce power while lowering its salinity. This is done by using salinity-gradient power production technologies. Among these technologies, pressure-retarded osmosis (PRO) is believed to be the most promising technology because of its higher energy density [22, 23] although efforts to improve technologies such as reverse electrodialysis (RED) are continuing [24, 25]. In PRO, two flow streams at different salinities are introduced into a module where a semi-permeable membrane selectively rejects salt molecules. The more concentrated stream is commonly referred to as the draw stream and the less concentrated one as feed. Because of the chemical potential difference, osmosis occurs and water is drawn from the feed to the draw side. The draw stream is pressurized before being sent into the module which retards the osmosis (hence the name pressure-retarded osmosis). The applied pressure difference is smaller than the osmotic pressure difference so that osmosis is allowed to occur. The draw stream leaving the module is run through a turbine to produce power. The power produced by the system is net positive because the flow rate of the draw is higher at the outlet due to osmosis.

Some researchers have studied coupling PRO to a desalination system [26, 27], but their analyses were limited to the salinity range of seawater reverse osmosis (SWRO) (brine salinity of about 70 g/kg). Prante et al. [28] considered a wide range of salinities, but their PRO model was set up in parallel flow configuration, which is always less efficient than the counterflow configuration [29], and the analysis used an average flux, which results in an inaccurate representation of the variations actually found in a module-scale system.

1.1. Objective

In this paper, we study the thermodynamic limits of the two types of processes outlined above, and their corresponding subsystems in order to understand how far current systems are from these limits and to guide attempts to improve these systems. While energy considerations alone are not sufficient to guide the choice between different systems, understanding the energetics of the different brine management processes is essential in understanding their operation. Although the two brine management technologies produce

different outputs, the underlying physics are so similar that they warrant tandem treatment. One process involves separation of salt and water whereas the other mixes salt and water in a controlled manner, and both can be analyzed with the same thermodynamic principles.

We first approach ZDD brine management method from a purely thermodynamic perspective. While several researchers have proposed ZDD-like systems for producing both water and salt from seawater and while several commercial plants have been built, a study outlining the thermodynamic limits on the work required for producing salt and water from seawater in a ZDD process is missing in the literature. ZDD is typically achieved using a series of sub-processes and technologies such as reverse osmosis (RO), ED, mechanical vapor compression (MVC) systems, multi-effect evaporators and crystallizers. An understanding of the performance limits of ZDD informs process designers and researchers on where current ZDD processes and sub-processes stand in terms of efficiency as well as the potential for improvement. To address these issues, a detailed analysis of the thermodynamic minimum work required for concentrating brine up to the saturation limit and the minimum work for subsequent crystallization for salt production are presented. In addition, we calculate the Second Law efficiency values of the state-of-the-art technologies used in industrial ZDD process to compare relative magnitude of energy input required for brine concentration and crystallization step.

For the salinity-gradient power generation method, we have performed an analysis from fundamental thermodynamic laws to understand the energetics of the coupling process. Based on this fundamental understanding, we expand our study to a practical power generation system using pressure-retarded osmosis (PRO) and quantify the energetic saving of adding PRO. We use nonlinear optimization to determine the best operating conditions, which results in general results (i.e., not restricted to a particular choice of operating conditions).

2. Blackbox systems

2.1. Salt production and zero-discharge desalination

In this section we present an analysis of the thermodynamic minimum work required for brine concentration as well as salt production. Figure 2 shows a blackbox diagram of a brine concentrator as well as a crystallizer. Feed enters the black box brine concentrator at a salinity s_f and mass flow rate $\dot{m}_\mathrm{f}$. The brine concentrator produces a pure product water stream with a mass flow rate $\dot{m}_\mathrm{p,bc}$ and a saturated brine stream with a mass flow rate $\dot{m}_\mathrm{b}$. The saturated brine stream enters the black box crystallizer where it is separated into a pure salt and pure product water stream of mass flow rates, $\dot{m}_\mathrm{p,crys}$ and $\dot{m}_\mathrm{s}$. In our analysis, the blackbox brine concentrator and blackbox crystallizer are work driven systems. Under reversible conditions, the work required would be the 'least work' thermodynamically possible, which for brine concentration and

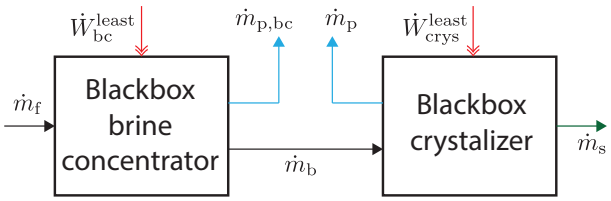

Figure 2: Flow diagram of reversible, blackbox brine concentration system and crystallizer.

crystallization we designate as $\dot{W}_{\mathrm{bc}}^{\mathrm{least}}$ and $\dot{W}_{\mathrm{crys}}^{\mathrm{least}}$, respectively. Thus, the least work for brine concentration is the least work for concentrating from a given feed salinity up to saturation, while the least work for crystallization is the least work for taking a saturated solution up to complete separation of water and salt [30].

To calculate the least work, the First and Second Laws of thermodynamics were applied to each blackbox. The resulting equations were then combined to express the least work required by each black box as a function of the specific Gibbs energy of the incoming and outgoing streams. For a reversible process, the entropy generation is zero. Thus, we get the thermodynamic least work required for brine concentration and crystallization given by Eqs. (1) and (2) under the assumption that the inlet and outlet streams have the same temperature and presssure.

$$\dot{W}_{\mathrm{bc}}^{\mathrm{least}} = \dot{m}_{\mathrm{p,bc}} g_{\mathrm{p,bc}} + \dot{m}_{\mathrm{b}} g_{\mathrm{b}} - \dot{m}_{\mathrm{f}} g_{\mathrm{f}} \tag{1}$$

$$\dot{W}_{\mathrm{crys}}^{\mathrm{least}} = \dot{m}_{\mathrm{p,crys}} g_{\mathrm{p,crys}} + \dot{m}_{\mathrm{s}} g_{\mathrm{s}} - \dot{m}_{\mathrm{b}} g_{\mathrm{b}} \tag{2}$$

where g is the specific Gibbs energy. The detailed derivation of Eq. (1) can be found in Mistry et al. [31]. Equation (2) was obtained by following the same methodology outlined by Mistry et al. [31]. Both Eq. (1) and Eq. (2) have been derived previously on a per mole basis by Van der Haam [32].

As can be seen, the final expressions for least work in Eqs. (1) and (2) are functions of the mass flow rates and the specific Gibbs energies (on a per mass basis) of streams entering and leaving the blackbox. The specific Gibbs energy of the feed, product and brine solution streams (on a per mass basis) are calculated using the activity coefficients of the sodium chloride and pure water components (on a per mole basis). The activity coefficients were obtained from an implementation by Thiel et al. [30, 33] of Pitzer's equations modeling the thermodynamics of aqueous electrolyte solutions [34–39]. Thiel et al. [30] found that aqueous NaCl serves as a reasonable surrogate for the property estimation in certain high salinity waters.

In Chapter 2 of his thesis, Van der Haam [32] had described the derivation of the least work of crystallization. Here, the methodology is presented in a simplified manner. Additionally, to the best of our knowledge,

the detailed results described here related to the least work of crystallization, have not been published. For these reasons, we have described below how the least work of crystallization was evaluated along with a detailed analysis and discussion of results for the least work for brine concentration and crystallization for varying feed inlet salinities.

Equation (2) can be expressed on a molar basis as:

$$\dot{W}_{\text{crys}}^{\text{least}} = \dot{N}_{\text{p, crys}}\bar{g}_{\text{p,crys}} + \dot{N}_{\text{s}}\bar{g}_{\text{s}} + \dot{N}_{\text{b}}\bar{g}_{\text{b}} \tag{3}$$

where $\bar{g}$ is the partial molar Gibbs energy of each stream and $\dot{N}$ refers to molar flow rate of each stream. The three streams are identified by the subscripts: 'p, crys' for the product water leaving the crystallizer, 'b' for the brine stream entering the crystallizer and 's' for the salt stream leaving the crystallizer. The expression for least work of crystallization can be further expressed as a function of the molar flow rates of sodium chloride and water in the brine stream as:

$$\dot{W}_{\text{crys}}^{\text{least}} = \dot{N}_{\text{H2O,b}}(\bar{g}_{\text{H2O,p,crys}} - \bar{g}_{\text{H2O,b}}) + \dot{N}_{\text{NaCl,b}}(\bar{g}_{\text{NaCl,s}} - \bar{g}_{\text{NaCl,b}}) \tag{4}$$

where $\dot{N}_{\text{H2O,b}}$ and $\dot{N}_{\text{NaCl,b}}$ are given by, $\dot{N}_{\text{H2O,b}} = \dot{m}_{\text{p}}/(M_{\text{H2O}})$ and $\dot{N}_{\text{NaCl,b}} = \dot{m}_{\text{s}}/(M_{\text{NaCl}})$. The molar masses of pure water (M_{H2O}) and sodium chloride (M_{NaCl}) are 18.02 g/mol and 58.44 g/mol respectively. $\bar{g}_{\text{H2O,p,crys}}$ and $\bar{g}_{\text{H2O,b}}$ are the partial molar Gibbs energies of pure water in the product and brine streams while $\bar{g}_{\text{NaCl,s}}$ and $\bar{g}_{\text{NaCl,b}}$ are the partial molar Gibbs energies of sodium chloride in the solid salt and aqueous brine streams.

From thermodynamic principles, at saturation, sodium chloride in the solid hydrous form is in equilibrium with the sodium chloride in the saturated solution. Thus, the partial molar Gibbs energies of solid sodium chloride and of sodium chloride in its saturated solution are equal:

$$\bar{g}_{\text{NaCl,s}} = \bar{g}_{\text{NaCl,sat}} \tag{5}$$

Now, Eq. (4), can be expressed as function of the activities of sodium chloride and water in the three streams as:

$$\dot{W}_{\text{crys}}^{\text{least}} = RT\left(\dot{N}_{\text{H2O,b}}\ln\frac{a_{\text{H2O,p,crys}}}{a_{\text{H2O,b}}} + \dot{N}_{\text{NaCl,b}}\ln\frac{a_{\text{NaCl,sat}}}{a_{\text{NaCl,b}}}\right) \tag{6}$$

where, R is the universal gas constant given by 8.3145 J/mol-K, T is the temperature in kelvin, which in this case is 298 K, and a refers to the activities of the components in a stream. For the crystallizer, the

incoming brine is assumed to be saturated, thus the equation further simplifies as:

$$\dot{W}_{\text{crys}}^{\text{least}} = RT\left(\dot{N}_{\text{H2O,sat}} \ln \frac{a_{\text{H2O,p,crys}}}{a_{\text{H2O,sat}}}\right) \tag{7}$$

Expressing $\dot{N}_{\text{H2O,sat}}$ as a function of the feed mass flow rate ($\dot{m}_{\text{f}}$) and feed salinity (s_{f}) into the brine concentrator, we get:

$$\dot{W}_{\text{crys}}^{\text{least}} = \frac{\dot{m}_{\text{f}} s_{\text{f}} RT}{1000}\left[\frac{1}{M_{H2O}}\left(\frac{1000}{s_{\text{sat}}} - 1\right) \ln \frac{a_{\text{H2O,p}}}{a_{\text{H2O,sat}}}\right] \tag{8}$$

Similarly, the above analysis can be applied to the combined control volumes of both the black box brine concentrator and black box crystallizer to obtain an expression for the total least work. The expression is similar to that given by Eq. (6):

$$\dot{W}_{\text{total}}^{\text{least}} = \dot{W}_{\text{bc}}^{\text{least}} + \dot{W}_{\text{crys}}^{\text{least}} = RT\left(\dot{N}_{\text{H2O,f}} \ln \frac{a_{\text{H2O,p}}}{a_{\text{H2O,f}}} + \dot{N}_{\text{NaCl,f}} \ln \frac{a_{\text{NaCl,sat}}}{a_{\text{NaCl,f}}}\right) \tag{9}$$

where, $a_{\text{H2O,p}}$ represents the activity of water in the pure product water, the value of which is the same in the product water streams from both the brine concentrator and crystallizer. The activities in the above equations were obtained as previously mentioned from an implementation of Pitzer's equations by Thiel et al. [30, 33].

2.1.1. Results

Figure 3 shows the results for the least work required to concentrate 1 kg/s of feed to saturation and then completely crystallize it for varying feed salinities. Least work is normalized by the mass flow rate of the feed into the brine concentrator ($\dot{m}_{\text{f}}$). Alternatively, the least work could be normalized by either the mass of the salt produced or by that of the water produced, depending typically on what is the desired substance. For the purpose of brine management, normalizing using the the feed mass flow rates is appropriate because one of the main aims of brine management is to reduce the mass of an incoming feed stream. The total least work required in general increases with the feed salinity, but as the feed becomes saturated, the total least work required decreases marginally. This trend results from competing effects in the least work of completely crystallizing saturated brine and the least work for concentrating brine to saturation. As feed salinity increases, the salt content for a fixed total feed mass increases proportionately, resulting in a corresponding linear increase in the least work for crystallization. The linear relationship of least work of crystallization with feed salinity can be inferred as well from Eq. (8). For brine concentration, as the feed salinity increases, two effects compete: the energy required to remove an incremental amount of water increases while the absolute amount of water needed to be removed to achieve saturation decreases. The former effect dominates initially

up to feed salinities around 120 g/kg, while for higher salinities the latter effect dominates.

For comparison, the ratio of the least work for concentrating feed until saturation to the total least work for complete separation is shown in Fig. 4. At a feed salinity of 100 g/kg, brine concentration contributes 50% of the total least work. This can also be seen in Fig. 3, where at a feed salinity of 100 g/kg, the least work for brine concentration and least work for crystallization cross over. It is evident from both of these figures that the least work for brine concentration until saturation and the least work for complete crystallization thereafter are comparable in the desalination range of feed salinities (35 g/kg to 120 g/kg), after which the least work of crystallization is dominant.

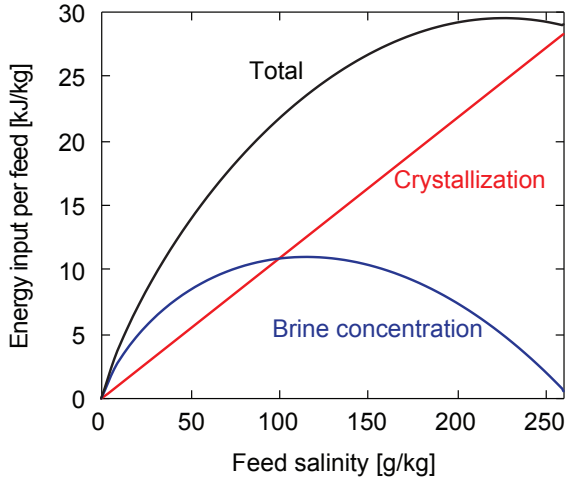

Figure 3: Least work per unit feed for brine concentration, crystallization and total energy consumption of ZDD at varying feed salinities.

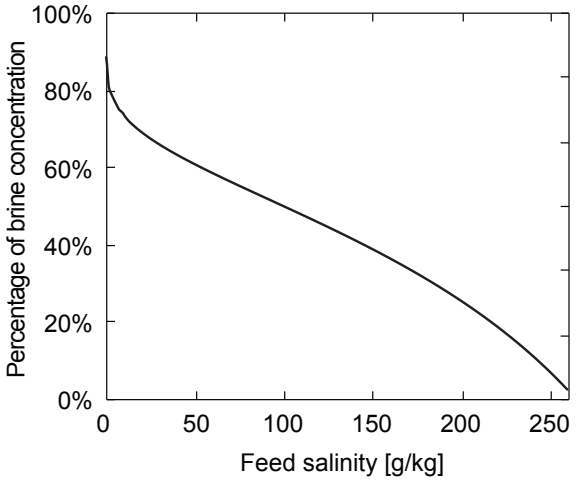

Figure 4: Percentage of brine concentration energy consumption in total ZDD process energy consumption.

To put the least work values in perspective, we calculated them at a specific feed salinity. For a feed

salinity of 35 g/kg, the least work for brine concentration until saturation is 6.94 kJ/kg-feed while the least work for complete crystallization is 3.81 kJ/kg-feed. Thus, brine concentration contributes to 64.5% of the total least work. Figure 5 shows the percentage of water mass remaining as 35 g/kg feed is concentrated until saturation. At saturation, approximately 90% of the original water mass has been removed through brine concentration. Crystallization separates the remaining 10% of original water mass. The last step of removing 10% of the original water mass requires 35.5% of the total least work. Thus, under ideal operating conditions, crystallization is a more work intensive step than brine concentration when viewed from a perspective of volume or mass reduction. However, crystallization is typically a thermally driven process. Because least work of crystallization represented here is the exergetic values, thermal energy input for crystallization has to be converted to its exergy so that it can be clearly compared with the performance limits of brine concentration.

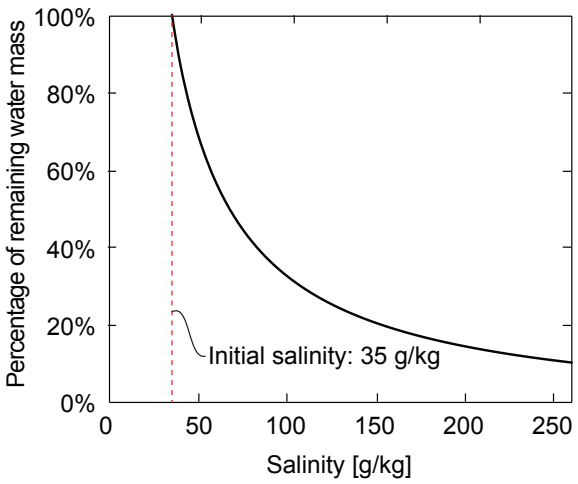

Figure 5: Percentage of remaining water mass as a solution is concentrated from an initial salinity of 35 g/kg up to saturation

For the benefit of readers in the desalination industry, the results for least work from Fig. 3 relevant to the salinity range for seawater desalination operation (35 g/kg to 120 g/kg feed salinities) were represented separately in Fig. 6. The figure further highlights that for typical operating conditions, the least work for brine concentration until saturation and the least work for crystallization thereafter are comparable in magnitude.

2.2. Power production from salinity gradients

In this section, we analyze salinity-gradient power production as a means of brine management. Thermodynamically, energy is required to separate salt from water. By reversing the process, energy can be generated when salt and water are mixed. Figure 7 shows two reversible, blackbox systems: one separating seawater into pure water and brine (denoted here as $\dot{m}_{\mathrm{p}}$ and $\dot{m}_{\mathrm{d,in}}$, respectively), and the other one mixing

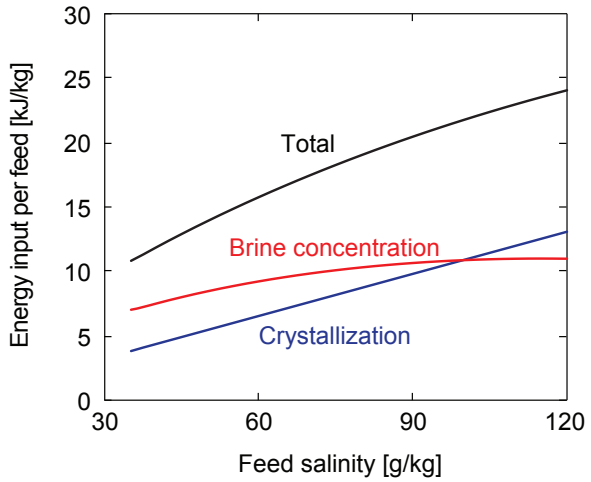

Figure 6: Least work per unit feed for brine concentration, crystallization and total energy consumption of ZDD in the salinity range relevant for seawater desalination.

the brine and pure water streams. A reversible desalination system requires the thermodynamic minimum amount of energy input, which is sometimes referred to as least work of separation [30, 40]. In this paper, the least work is denoted by $\dot{W}_{\rm in}^{\rm least}$. The reversible mixer generates the maximum amount of energy by mixing the streams at the given salinities because there is no entropy generation and associated lost work [41]. By virtue of being reversible systems, the least work ($\dot{W}_{\rm in}^{\rm least}$) is exactly the same as that of energy produced from mixing ($\dot{W}_{\rm out}^{\rm max}$).

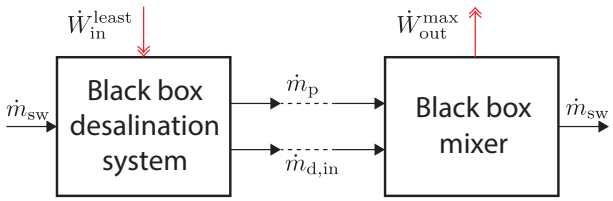

Figure 7: Flow diagram of reversible, blackbox desalination system and mixer.

Using the system configuration outlined in Fig. 7, generating more energy from mixing than the least work violates the Second Law of thermodynamics. However, if a different relatively purer stream at an appropriate salinity and flow rate, $\dot{m}_{\rm f,in}$, is used for energy generation, more energy can be generated than the separation energy without violating the Second Law. We show this using a purely thermodynamic construct. Figure 8 shows a schematic diagram of this process.

The system outlined in Fig. 8 consists of the same two blackbox systems: one for desalination and another for power production. As these systems are analyzed by the control-volume method, what is happening inside the blackbox is not relevant. The First and Second Laws of thermodynamics can be applied to each system. Following the same approach as in Sec. 2 to combine the First and Second Law equations results in Eqs. (10)

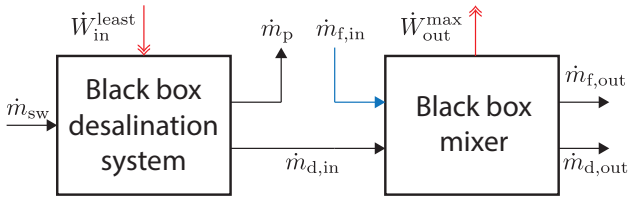

Figure 8: Flow diagram of reversible, blackbox desalination system and a mixer utilizing an independent flow stream ($\dot{m}_{\text{f,in}}$).

and (11) for desalination and power production systems, respectively:

$$\dot{W}_{\text{in}}^{\text{least}} = \dot{m}_{\text{p}} g_{\text{p}} + \dot{m}_{\text{d,in}} g_{\text{d,in}} - \dot{m}_{\text{sw}} g_{\text{sw}} \tag{10}$$

$$\dot{W}_{\text{out}}^{\text{max}} = \dot{m}_{\text{d,in}} g_{\text{d,in}} - \dot{m}_{\text{d,out}} g_{\text{d,out}} + \dot{m}_{\text{f,in}} g_{\text{f,in}} - \dot{m}_{\text{f,out}} g_{\text{f,out}} \tag{11}$$

Equations (10) and (11) depend on the magnitude of the mass flow rates. Working with normalized quantities circumvents this dependence. To normalize the equations, we define three dimensionless variables:

$$\text{RR}_{\text{desal}} \equiv \frac{\dot{m}_{\text{p}}}{\dot{m}_{\text{sw}}} \tag{12}$$

$$\text{RR}_{\text{power}} \equiv \frac{\dot{m}_{\text{d,out}} - \dot{m}_{\text{d,in}}}{\dot{m}_{\text{f,in}}} = \frac{\dot{m}_{\text{f,in}} - \dot{m}_{\text{f,out}}}{\dot{m}_{\text{f,in}}} \tag{13}$$

$$\text{MR} \equiv \frac{\dot{m}_{\text{d,in}}}{\dot{m}_{\text{f,in}}} \tag{14}$$

where RR_{desal} and RR_{power} are the recovery ratios of the desalination and power generation (mixer) systems, respectively. They are ratios of the permeation flow rate to the feed flow rate. MR specifies the flow rate ratio of the two streams in the mixer. Using the definitions of these dimensionless variables, Eqs. (10) and (11) can be recast into following forms by dividing both sides by $\dot{m}_{\text{p}}$:

$$w_{\text{in}}^{\text{least}} = g_{\text{p}} + \left(\frac{1 - \text{RR}_{\text{desal}}}{\text{RR}_{\text{desal}}} \right) g_{\text{d,in}} - \frac{1}{\text{RR}_{\text{desal}}} g_{\text{sw}} \tag{15}$$

$$w_{\text{out}}^{\text{max}} = \left(\frac{1 - \text{RR}_{\text{desal}}}{\text{RR}_{\text{desal}}} \right) \left[g_{\text{d,in}} - \left(\frac{\text{RR}_{\text{power}} + \text{MR}}{\text{MR}} \right) g_{\text{d,out}} + \frac{1}{\text{MR}} g_{\text{f,in}} - \left(\frac{1 - \text{RR}_{\text{power}}}{\text{MR}} \right) g_{\text{f,out}} \right] \tag{16}$$

where w refers to specific work values (i.e., normalized by $\dot{m}_{\text{p}}$). Both $w_{\text{in}}^{\text{least}}$ and $w_{\text{out}}^{\text{max}}$ have dimensions of

energy per unit mass of product water. A commonly used dimension for the specific energy is energy per unit volume of product water. Thus, $w_{\mathrm{in}}^{\mathrm{least}}$ and $w_{\mathrm{out}}^{\mathrm{max}}$ are multiplied by the pure water density (ρ_{p}) to convert the dimensions ($E_{\mathrm{in}}^{\mathrm{least}} = w_{\mathrm{in}}^{\mathrm{least}} \rho_{\mathrm{p}}$). The resulting specific energy variables are designated as $E_{\mathrm{in}}^{\mathrm{least}}$ and $E_{\mathrm{out}}^{\mathrm{max}}$ expressed in kWh/m^3.

Figure 9 shows specific, least energy of desalination ($E_{\mathrm{in}}^{\mathrm{least}}$) and maximum energy production ($E_{\mathrm{out}}^{\mathrm{max}}$) as a function of MR. Seawater properties are used to model the seawater and brine [42]. For this specific case, salinities were chosen to represent a typical seawater reverse osmosis (SWRO) system; that is, $s_{\mathrm{sw}} = 35$ g/kg, $s_{\mathrm{d,in}} = 70$ g/kg. Also purer $\dot{m}_{\mathrm{f,in}}$ stream has salinity ($s_{\mathrm{f,in}}$) of 1 g/kg.

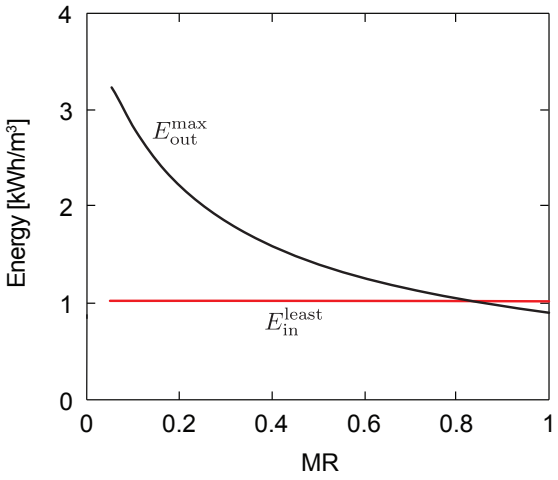

Figure 9: Least work of desalination ($E_{\mathrm{in}}^{\mathrm{least}}$) and the maximum energy generated from mixing ($E_{\mathrm{out}}^{\mathrm{max}}$) per volume of pure water produced from desalination. For MR below about 0.8, more energy is generated by the mixing stage than is required for the desalination stage. In this plot, $s_{\mathrm{sw}} = 35$ g/kg, $s_{\mathrm{d,in}} = 70$ g/kg, $s_{\mathrm{f,in}} = 1$ g/kg, $\mathrm{RR}_{\mathrm{desal}} = 0.5$, and $\mathrm{RR}_{\mathrm{power}} = 0.9$ are used.

More energy can be produced than required for the desalination energy consumption when MR is smaller than about 0.8. Recalling the definition of MR (Eq. (14)), $\dot{m}_{\mathrm{f,in}}$ has to be larger than $\dot{m}_{\mathrm{d,in}}$. This trend can be understood with the aid of exergy. When MR is lowered, $\dot{m}_{\mathrm{f,in}}$ is effectively increased, which corresponds to an increase in the exergy input to the system. Therefore, more work can be generated. The flow rate and salinity of this stream are completely independent of the desalination system because changing either one does not affect the desalination process. This additional degree of freedom enables more energy to be generated than the least work input without violating the Second Law of thermodynamics.

3. Process-specific implementations

3.1. Zero-discharge desalination

In this section, we analyze a representative state-of-the-art real world implementation of zero-discharge desalination (ZDD) system, which consists of brine concentration and crystallization steps.

To quantify how close the practical systems are to the thermodynamic limit, we calculated their Second Law efficiencies. The Second Law efficiency for a chemical separation system is defined as the ratio of the least exergy of separation to the exergy input to the system:

$$\eta_{II} \equiv \frac{\text{least exergy of separation}}{\text{exergy input}} \tag{17}$$

The least exergy of separation is equal to the least work of separation ($\dot{W}_{\text{in}}^{\text{least}}$) which is a function of the salinities of the process streams irrespective of the type of energy input [31]. For the separation processes of brine concentration and crystallization, the least work was given in Eqs. (1) and (2), respectively for which the inlet and outlet streams are assumed to have the same temperatures, T_0. The exergy input to the system depends on the definition of the system and its control volume. Following the approach of [31], the First and Second Laws of Thermodynamics can be applied to the system shown in Fig. 10.

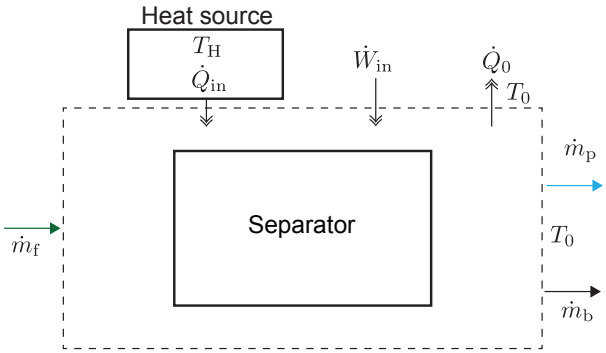

Figure 10: A control volume for a separator powered by work and/or heat input.

$$\dot{m}_{\text{f}}h_{\text{f}} - \dot{m}_{\text{b}}h_{\text{b}} - \dot{m}_{\text{p}}h_{\text{p}} + \dot{Q}_{\text{H}} - \dot{Q}_0 + \dot{W}_{\text{in}} = 0 \tag{18}$$

$$\dot{m}_{\text{f}}s_{\text{f}} - \dot{m}_{\text{b}}s_{\text{b}} - \dot{m}_{\text{p}}s_{\text{p}} + \frac{\dot{Q}_{\text{H}}}{T_{\text{H}}} - \frac{\dot{Q}_0}{T_0} + \dot{W}_{\text{in}} + \dot{S}_{\text{gen}} = 0 \tag{19}$$

where $\dot{W}_{\text{in}}$ is the net rate of work transfer into the system, T_0 is the temperature of the environment, T_{H} is the temperature of the source from which the heat transfer $\dot{Q}_{\text{in}}$ into the system occurs. Note that the control volume is treated as being sufficiently large that the process streams (i.e., feed, pure water, brine or salt) all enter and leave at the dead state temperature (T_0) and pressure (P_0), which requires heat transfer to the environment, ($\dot{Q}_0$). (For discussion of the control system boundary, see [40], Sec. 2.1.) For the system in Fig. 10, $\dot{Q}_0$ crosses the system boundary (or control surface) at T_0. By eliminating $\dot{Q}_0$ and substituting

the specific Gibbs energy, Eqs. (18) and (19) can be combined and rearranged into:

$$\dot{W}_{\text{in}} + \dot{Q}_{\text{H}} \left(1 - \frac{T_0}{T_{\text{H}}}\right) = \dot{m}_{\text{p}} g_{\text{p}} + \dot{m}_{\text{b}} g_{\text{b}} - \dot{m}_{\text{f}} g_{\text{f}} + T_0 \dot{S}_{\text{gen}} \tag{20}$$

The left-hand side of Eq. (20) is the exergy input into the system required for the desired separation of the process streams into the specified salinities at the dead state temperature and pressure. The second term, $\dot{Q}_{\text{H}} \left(1 - \frac{T_0}{T_{\text{H}}}\right)$, is the exergetic value of $\dot{Q}_{\text{H}}$. The scalar multiplier $\left(1 - \frac{T_0}{T_{\text{H}}}\right)$ is the Carnot efficiency (less than unity), which accounts for the fact that a heat input has a lower exergetic value than a work input. The conversion of heat to its exergetic value is conceptually achieved by operating a reversible heat engine between the heat source at T_{H} and heat sink at T_0. The heat engine converts $\dot{Q}_{\text{H}}$ reversibly into work with a magnitude equal to the exergetic value of the heat input.

Substituting the least work and the left-hand side of Eq. (20) into Eq. (17) results in a definition of Second Law efficiency of separation system which takes energy inputs in the form of work and/or heat.

$$\eta_{II} = \frac{\dot{W}_{\text{in}}^{\text{least}}}{\dot{W}_{\text{in}} + \dot{Q}_{\text{in}} \left(1 - \frac{T_0}{T_{\text{H}}}\right)} \tag{21}$$

Second Law efficiency ranges from 0 to 1; completely reversible systems have a Second Law efficiency equal to unity. A low Second Law efficiency indicates that there is a high potential to improve the system, in other words, to effect greater separation with the same energy inputs.

For an actual work-driven brine concentrator and thermal-energy driven crystallizer, the Second Law efficiency would be, respectively:

$$\eta_{II,\text{bc}} = \frac{\dot{W}_{\text{bc}}^{\text{least}}}{\dot{W}_{\text{bc}}} \tag{22}$$

$$\eta_{II,\text{crys}} = \frac{\dot{W}_{\text{crys}}^{\text{least}}}{\dot{Q}_{\text{crys}} \left(1 - \frac{T_0}{T_{\text{H}}}\right)} \tag{23}$$

Now that we have the definition of Second Law efficiency, we can evaluate specific technologies for brine concentration and crystallization. Seawater feed is first concentrated from 35 g/kg to saturation using a single-effect mechanical vapor compression (MVC) system followed by crystallization using a 6-effect thermal evaporator. For the brine concentration step, a two-effect MVC system was also studied. The technologies that we chose are to the best of our knowledge, the most frequently used and state-of-the-art technologies in the industry. While MVC systems can be operated with greater than two effects, systems with greater than two effects are not common.

Figure 11 shows the schematic diagram of both systems and their control volumes (dashed box). To be consistent with the control volume analysis in Fig. 10, all the streams in Fig. 11 enter and leave at dead state temperature and pressure. As a result, when the brine stream leaves the control volume on the left-hand side and reenters the control volume on the right-hand side, the temperature is T_0. This is also consistent with the multi-effect evaporator data obtained from [11] which has streams entering at a temperature of T_0. In practice, the stream leaving the regenerator of the MVC system does not need to be cooled all the way to T_0 before reentering the crystallizer. But this cooling is small compared to the heat input ($\dot{Q}_{\text{in}}$) in any case.

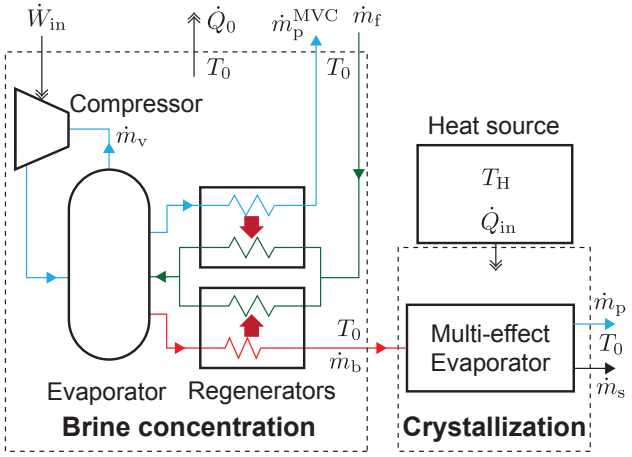

Figure 11: Mechanical vapor compression (MVC) system for brine concentration and thermal multi-effect evaporator for crystallization and their control volumes. The control volumes are sufficiently large that all streams enter and leave at dead state temperature and pressure. The multi-effect evaporator is shown as blackbox because we use literature data instead of modeling it.

3.1.1. Mechanical Vapor Compression Brine Concentration

The work and heat transfer rates required for the MVC system and the evaporator were obtained from modeling work and from the literature, respectively. An existing model for MVC [43] was used to calculate the work required to concentrate seawater from 35 g/kg to saturation using a single-effect MVC system. The model itself is based on an earlier work by El-Dessouky [44]. Properties for aqueous sodium chloride were obtained from an implementation of Pitzer's equations [37]. Parameters used for modeling as well as the results are given in Table 1. The efficiency of the compressor (η_{comp}) was set to 70% and the evaporator temperature (T_{evap}) was set to 346 K. The terminal temperature difference (ΔT_{TTD}) in the evaporator and the pre-heaters was 3 K. The brine and the product water streams were assumed to leave the pre-heater at the same temperature [44]. The streams were found to leave the pre-heaters around 15 K above the environment temperature T_0. In stand-alone MVC systems, typically, the exergy within these streams are not extracted, and heat transfer to the environment is allowed so that the streams eventually reach a temperature T_0. This corresponds to the heat transfer rate of $\dot{Q}_0$, depicted in Fig. 11. The actual work required to operate the

single-effect MVC system per feed mass flow rate was 78.8 kJ/kg while the least work was 6.7 kJ/kg leading to a Second Law efficiency of 8.5%. The Second Law efficiency value of 8.5% obtained here also corresponds approximately to the efficiency values reported by Thiel et al. [30].

MVC brine concentration systems are also deployed in "forward feed multiple effect" configurations where the thermal energy obtained from condensation of product water in one effect is used to evaporate feed and generate vapor to be condensed in a subsequent effect. To ascertain the performance improvement from adding effects, a two-effect forward feed MVC system was also modeled. The model combined elements from the single-effect MVC system model described previously with a multi-effect distillation system model developed earlier by El-Dessouky [44]. The input conditions, constraints and assumptions used in the two-effect model were identical to those used in the single-effect model. To make a fair comparison, the evaporator in the first effect of the two-effect system was maintained at a temperature of 346 K, the same as the evaporator temperature in the one-effect system. The two-effect model was validated against the results published by Thiel et al. [30]. Thiel et al. found that the Second Law efficiency of a two-effect MVC system for concentrating produced water brine from 150 g/kg to 260 g/kg was around 30%. The model developed here gave approximately the same efficiency under those conditions. The validated two-effect MVC model was then used to calculate the work required to concentrate seawater from 35 g/kg to saturation. The results are shown in Table 1. The actual work required to operate the two-effect MVC system per feed mass flow rate was 57.3 kJ/kg while the least work was 6.7 kJ/kg leading to a Second Law efficiency of 11.6 %.

Table 1: MVC model parameters and results

MVC parameters	Unit	Value	
Inputs			
$\dot{m}_{\mathrm{f}}$	kg/s	1	
s_{f}	g/kg	35	
s_{b}	g/kg	250	
η_{comp}		70%	
T_{evap}	K	346	
ΔT_{TTD}	K	3	
$w_{\mathrm{bc}}^{\mathrm{least}}$	kJ/kg	6.7	
Outputs			
		1-effect	2-effect
w_{bc}	kJ/kg	78.8	57.3
η_{II}		8.5%	11.6 %

3.1.2. Multi-effect thermal evaporator crystallizer

Performance data for a 6-effect thermal evaporator that completely separates saturated solution into pure salt and water was obtained from Sedivy [11]. Table 2 summarizes the data from Sedivy [11] as well as the

outputs. Sedivy had reported the thermal energy input to the system q_{crys} and the temperature at which the input is occuring (T_{H}). The Second Law efficiency of the thermal evaporator crystallizer was calculated using Eq. (23). From the procedure outlined in Sec. 2, the least work for crystallization ($w_{\text{crys}}^{\text{least}}$) was found to be 29.2 kJ/kg. The calculated Second Law efficiency of the thermal evaporator was 24.4%. The data in the literature did not report electric work required for pumping and other peripheral operation. Compared to the exergy of the thermal input, the parasitic power requirements were assumed to be neglegible. This assumption is consistent with models for thermal desalination systems in the literature [40].

Table 2: Thermal evaporator parameters and results

Evaporator parameters	Unit	Value
Inputs		
$\dot{m}_{\text{f}}$	kg/s	1
s_{b}	g/kg	250
q_{crys}	kJ/kg	351 [11]
T_{H}	K	453 [11]
T_0	K	298
$w_{\text{crys}}^{\text{least}}$	kJ/kg	29.2
Outputs		
η_{II}		24.4%

The heat source temperature used in this study is 453 K. Because multi-effect evaporator's highest temperature is typically maintained at 343 K, a temperature difference of 110 K is driving the heat transfer from which the multi-effect evaporator system receives the heat input. This generates significant amount of entropy, reducing the Second Law efficiency.

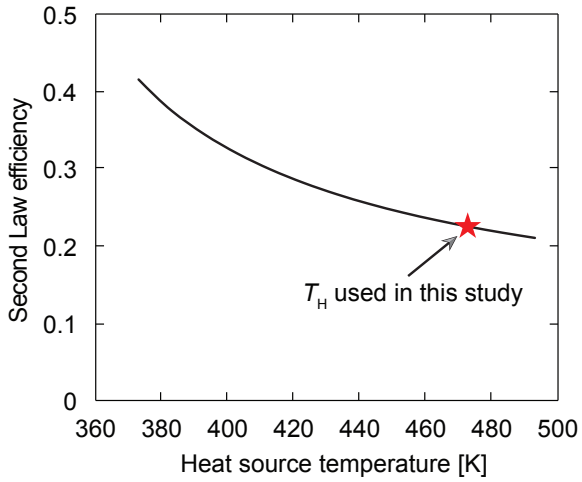

Figure 12: Second Law efficiency as a function of the heat source temperature.

Figure 12 shows a hypothetical scenario where the heat source temperature is varied while the same

quantity of heat input is used. The Second Law efficiency of the multi-effect evaporator system increases from 24.4% to 41.4% as the heat source temperature decreases from 453 K to 373 K. Therefore, when low grade thermal energy is available (e.g., low pressure steam), it is thermodynamically much more favorable to utilize it. Smaller temperature difference entails larger heat exchanger area in order to maintain the same quantity of heat transfer. For the crystallization process, corrosion resistant metal alloys and metals such as titanium are used for heat exchange surfaces. Titanium in particular has been operationally found to be a very reliable material, resistant to corrosion and erosion at both high salinities and temperatures [45, 46]. However, such materials are expensive, and increasing the heat exchanger area may significantly increase the capital cost. Therefore, an economic optimum should be used to decide the optimal temperature of the heat source. Another way to look at this conclusion is that using cheaper material that is resistant to corrosion and erosion has the potential to increase the Second Law efficiency by lowering the top temperature through an increase of heat exchanger area, and we believe that identifying a cheaper material is worth further research.

A comparison of the final calculated Second Law efficiencies of the MVC brine concentrators and the multi-effect evaporator crystallizer is shown in Fig. 13. The least efficient system was the single-effect MVC brine concentrator with a Second Law efficiency of 8.5%. The two-effect MVC system was marginally better with an efficiency of 11.6%, while the six-effect thermal evaporator performed more than twice as well with an efficiency of 24.4%. The previous discussion highlighted how the efficiency of the crystallizer could be increased further by increasing the heat transfer area and reducing the temperature at which heat is being transferred to the crystallizer. The analysis makes it clear that research efforts on improving the energy efficiency of zero-discharge desalination should focus on the "brine concentration" step rather than the "crystallization" step given the much more significant room for improvement in the former.

3.1.3. Efficiency gains from adding more effects to an MVC system

A natural question that follows from the above analysis is: could increasing the number of effects in an MVC system make brine concentration as efficient as crystallization? We focused our analysis on single-effect and two-effect MVC systems because to the best of our knowledge they are the most deployed configurations globally. However, MVC systems with greater than two "forward feed" effects also exist. Our analysis of single-effect and two-effect MVC systems showed that adding any more effects would improve the efficiency only incrementally. To confirm this, the two-effect model we made was extended to three effects keeping all other conditions the same. We found that for a three-effect system, the Second Law efficiency was 12.9%, corresponding to a 1.3% increase in efficiency as compared to the two-effect system. In comparison, moving from a one-effect to a two-effect system had increased the Second Law efficiency by 3.1%. Our model revealed

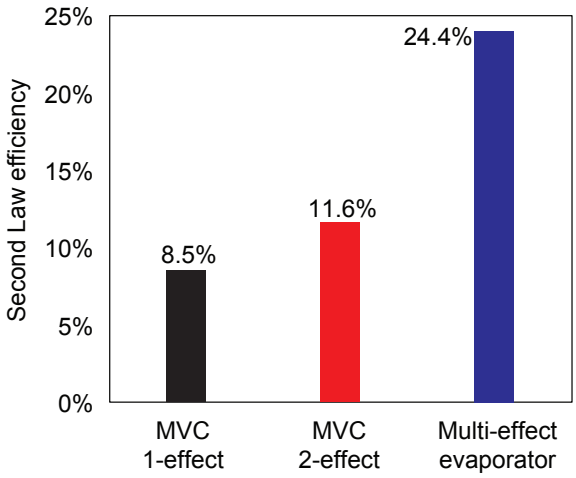

Figure 13: Second law efficiency of single-effect and two-effect mechanical vapor compression (MVC) brine concentrators and of a multi-effect evaporator (6-effect).

interesting conceptual insights that explained the decreasing returns per effect. With additional effects, the mass flow rate of vapor through the compressor reduced proportionately. However, the compression ratio across the compressor increased to account for the evaporator terminal temperature difference and boiling point elevation contribution of each additional effect. The overall effect was that the compressor work reduced only marginally with each additional effect. Extending the trend seen in Second Law efficiency values with the number of effects, we estimated that the Second Law efficiency of a six-effect MVC system would be around 14%, far lower than the 24% seen for a six-effect thermal crystallizer.

3.2. Pressure-retarded osmosis

In Sec. 2.2 we have seen that it is possible to generate more energy than what is needed for desalination. We can apply the same thermodynamic framework to a practical energy generation system. One of the most promising systems to harness salinity-gradient power is pressure-retarded osmosis (PRO). A schematic diagram of PRO coupled with a desalination system is shown in Fig. 14.

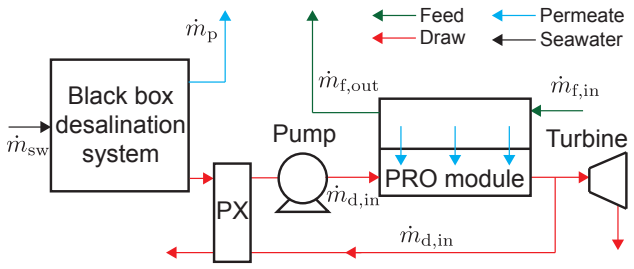

Figure 14: Schematic diagram of PRO coupled with a desalination system. PX refers to a pressure exchanger.

We use the same blackbox system for desalination because we want the results to be as general as

possible without being constrained to a particular desalination technology. However, in this section we will not assume the blackbox desalination system in Fig. 14 to be reversible; instead, we apply a value representative of state of the art SWRO systems. We do this to avoid combining a reversible input with an irreversible output. Finite difference method was used to numerically model the PRO system in counterflow configuration. By using the finite difference method, the transport equations reduce to differences instead of the original partial differential equations for the energy and mass balances. The PRO module is divided into a number of computational cells, which have to be solved simultaneously. These nonlinear equations were solved using Engineering Equation Solver (EES), which is a simultaneous equation solver based on Newton's method [47]. The modeling approach follows Chung et al. [48] and is summarized here.

At a high level, the ultimate goal of the PRO model is the calculation of the power production. The local reverse salt flux and the water flux at any axial location (x) can be calculated using Eqs. (24) and (25), respectively [48]:

$$J_{\mathrm{p}}(x) = A\left\{\pi_{\mathrm{d,m}}(x) - \pi_{\mathrm{f,m}}(x) - \left[P_{\mathrm{d}}(x) - P_{\mathrm{f}}(x)\right]\right\} \tag{24}$$

$$J_{\mathrm{salt}}(x) = B\rho\left[s_{\mathrm{d,m}}(x) - s_{\mathrm{f,m}}(x)\right] \tag{25}$$

where A is the membrane permeability, B is the solute permeability coefficient, J is the flux, $s_{\mathrm{d,m}}$, P_{d} and P_{f} are hydraulic pressures of the feed and draw streams, ρ is the density of water, and π is the osmotic pressure, and $s_{\mathrm{f,m}}$ are the salinities at the membrane surface on the draw and feed sides. These salinity values account for the concentration polarization as shown in Eqs. (26) and (27), respectively [49]:

$$s_{\mathrm{d,m}} = s_{\mathrm{d,b}}\exp\left(-\frac{J_{\mathrm{p}}}{\rho k}\right) - \frac{B\left(s_{\mathrm{d,m}} - s_{\mathrm{f,m}}\right)}{J_{\mathrm{p}}}\left[1 - \exp\left(-\frac{J_{\mathrm{p}}}{\rho k}\right)\right] \tag{26}$$

$$s_{\mathrm{f,m}} = s_{\mathrm{f,b}}\exp\left(\frac{J_{\mathrm{p}}S}{\rho D}\right) - \frac{B\left(s_{\mathrm{d,m}} - s_{\mathrm{f,m}}\right)}{J_{\mathrm{p}}}\left[\exp\left(\frac{J_{\mathrm{p}}S}{\rho D}\right) - 1\right] \tag{27}$$

where S, k and D are the structural parameter, the mass transfer coefficient, and the diffusion coefficient of NaCl in water. The mass transfer coefficient and the pressure drop in the flow channel can be calculated using the correlations by Schock and Miquel [50] as shown in Eqs. (28) and (29):

$$\mathrm{Sh} = 0.065\,\mathrm{Re}^{0.875}\mathrm{Sc}^{0.25} \tag{28}$$

$$f = 6.23\,\mathrm{Re}^{-0.3} \tag{29}$$

The power production from the turbine-generator assembly is:

$$\dot{W}_{\mathrm{PRO}} = \frac{\dot{m}_{\mathrm{p}}}{\rho}\left[P_{\mathrm{d}}\left(L\right) - P_{\mathrm{o}}\right] \tag{30}$$

where $P_{\mathrm{d}}(L)$ is the hydraulic pressure of the draw stream at the draw exit and P_{o} is the pressure of ambient state assuming the turbine discharge pressure is the same as the ambient pressure. In the PRO literature, the expression $\dot{W}_{\mathrm{PRO}} = JA_{\mathrm{m}}\Delta P$ is commonly used to calculated the power production, where A_{m} is the total membrane area [22, 23, 51]. However, this expression only applies for a zero-dimensional system where axial variation of the pressure and the osmotic driving force is negligible. For a module scale system, only the pressure at the end of the draw channel (i.e., $P_{\mathrm{d}}(L)$) is relevant for power production.

In specifying the operating conditions, a functional form (dimensional) of the power production equation is useful. $\dot{W}_{\mathrm{PRO}}$ (the dependent variable) is a function of 6 variables: the minimum water flux (J_{min}), the hydraulic pressure of the draw stream (P_{d}), the flow rate ratio (MR) and the velocity (v) of either stream [48]:

$$\dot{W}_{\mathrm{PRO}} = f(s_{\mathrm{d,in}}, s_{\mathrm{f,in}}, J_{\mathrm{min}}, v, P_{\mathrm{d}}, \mathrm{MR}) \tag{31}$$

In this study, the feed salinity ($s_{\mathrm{f,in}}$) is fixed at 1 g/kg, and the draw salinity ($s_{\mathrm{d,in}}$) is the independent variable (i.e., plotted as an abscissa). Specifying the velocity of one steam (either draw or feed) is sufficient because the other stream's velocity is determined by mass balance. The output power strongly depends on the choice of operating conditions. In order to generate general results, a wide range of operating conditions should be considered. One possible solution is using multi-variable optimization. In this paper, 3 variables (P_{d}, v and MR) were chosen such that the power input (E_{p}) is minimized. J_{min} was not used in the optimization because E_{p} is minimized as J_{min} approaches zero, which is clearly not economical as it implies infinite membrane area. Instead, several values of J_{min} were used to model practical systems. In addition, we included $J_{\mathrm{min}} = 0$ L/m^2-hr as a limiting case. For optimization, the conjugate gradient method was used [47]. Figure 15 summarizes the computational flow of the combined PRO and desalination system.

Because the available seawater properties correlations [42] have a maximum salinity level of 120 g/kg, we chose aqueous NaCl properties based on Pitzer's equations [37] to accurately model the effect of salinity on the osmotic driving force.

Since we are interested in a PRO system coupled with desalination, the metric of interest should quantify the energetic benefit of adding PRO to the desalination system. The net energy input to the coupled system

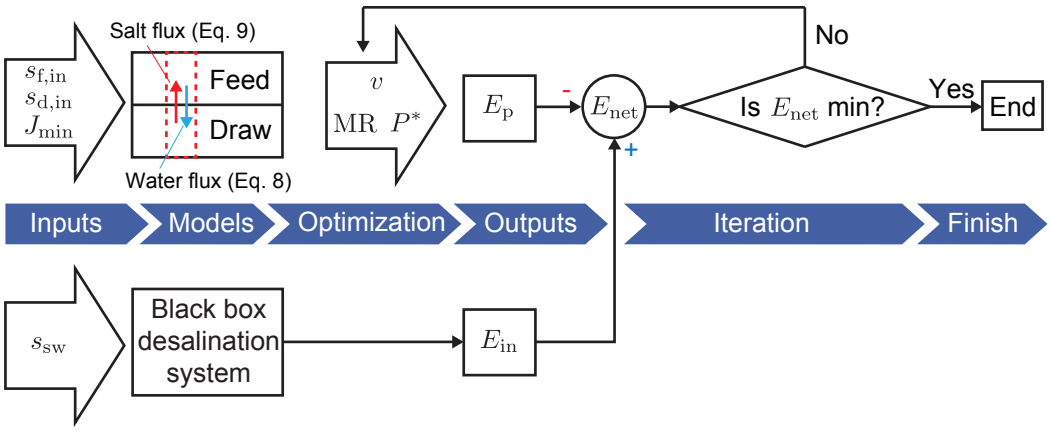

Figure 15: Flowchart of the computational model.

normalized by the pure water production from desalination represents the energy savings. However, in order to avoid directly comparing the irreversible energy output from PRO to the reversible energy input to the desalination system we need to estimate the energy input to the desalination system. The state-of-the-art seawater reverse osmosis (SWRO) systems have energy consumptions about 3–4 kWh/m^3 (normalized by pure water produced) of which about 1 kWh/m^3 is used for pretreatment [52]. This corresponds to a Second Law efficiency value of about 30% [40, 53]. In general, the Second Law efficiency of an RO system depends on the feed salinity in a nontrivial manner. Second Law efficiency increases with feed salinity up to about 200 g/kg then decreases with further increase in feed salinity, as discussed by Thiel et al. [30]. According to Eq. (21), the energy input to the desalination system can be approximated as $E_{\rm in} = E_{\rm in}^{\rm least}/\eta_{II}$. Then the net energy input to the integrated desalination and PRO system is given by Eq. (32).

$$E_{\rm net} \equiv E_{\rm in} - E_{\rm p} \tag{32}$$

where $E_{\rm p}$ is the PRO power normalized by the volume of desalination pure water production (i.e., $E_{\rm p} \equiv \dot{W}_{\rm PRO}\,\rho/\dot{m}_{\rm p}$). The net energy is normalized by the pure water production ($\dot{m}_{\rm p}$) because $\dot{m}_{\rm p}$ is the final product of the entire system. This normalization is useful because we can directly compare $E_{\rm net}$ to the desalination energy consumption.

Figure 16 shows the net energy consumption without PRO and with PRO for three levels of $J_{\rm min}$. As $J_{\rm min}$ increases, the system size decreases. In terms of economics, the whole cost of the system has to be minimized, which means that both capital cost and energetic cost should be accounted for. Energetic cost is minimized as $J_{\rm min}$ approaches zero whereas capital cost is minimized as $J_{\rm min}$ is maximized. Therefore, an economic optimum exists at an intermediate value of $J_{\rm min}$. Because PRO is not a well-established technology, it is hard to determine what value of $J_{\rm min}$ corresponds to an economic optimum. If we infer from a representative

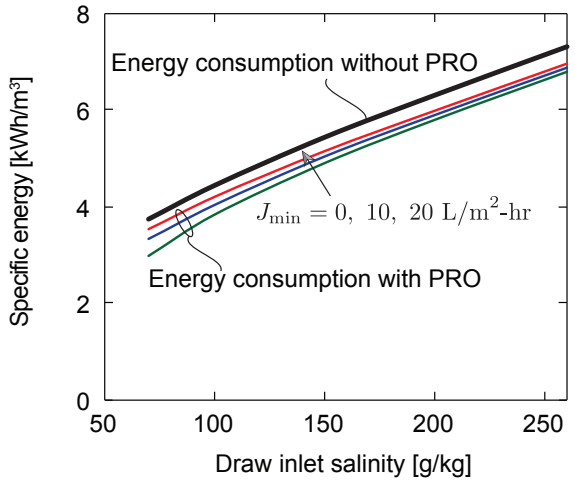

Figure 16: Specific energy consumption for desalination system without coupled PRO and with PRO.

reverse osmosis (RO) average flux 14 L/m^2-hr [52], the practical $J_{\min}$ value may lie between 10 and 20 L/m^2-hr. Along with the $J_{\min}$ values of 10 and 20 L/m^2-hr, Fig. 16 also shows the 0 L/m^2-hr case. We used a flux of 0.001 L/m^2-hr to approximate 0 L/m^2-hr in our numerical models.

For the case with $J_{\min} = 10$ L/m^2-hr, energy saving by adding the PRO unit is uniform over a wide range of salinities. For example, 0.42 and 0.43 kWh/m^3 of energy saving are possible with the $J_{\min} = 10$ L/m^2 system for 70 and 260 g/kg draw salinity, respectively. This corresponds to 6 and 11% of the desalination energy input (E_{in}). For the $J_{\min} = 0$ L/m^2-hr case, more energy saving is possible when the draw salinity is lower. The opposite trend is observed for $J_{\min} = 20$ L/m^2-hr case. This is because PRO power increases more with draw salinity when the minimum flux is higher.

For all the cases, energy saving is not significant, as shown in Fig. 16. PRO's energy saving is not very sensitive to the minimum flux. In particular, when the draw salinity is high, the net energy consumption tends to converge. This trend suggests that large minimum flux values can be used without significant energetic penalty. Because capital expenditure (CapEx) is the dominant cost factor for PRO [48], increasing the minimum flux (or decreasing the system size) can be an effective way to reduce the overall cost. Ultimately, the savings from operating expenditure (OpEx) in the form of energy reduction should be compared to the additional CapEx of the PRO unit to determine the economic viability of coupling PRO to a desalination system.

3.2.1. Osmotic driving force

Because the energy saving from the PRO unit is not significant (6–11% of the desalination energy), one natural way to increase the energy saving is by increasing the system size of the PRO unit, which reduces the overall driving force within the system, which in turn reduces the irreversibilities. For this study, increasing

the system size is equivalent to decreasing the minimum flux, $J_{\min}$. As shown in Fig. 16, when $J_{\min}$ is reduced from 10 to 0 L/m^2-hr, the energy saving is only slightly increased. This indicates that the membrane area is not utilized in an effective manner. In other words, the osmotic driving force within the PRO module is not well-distributed.

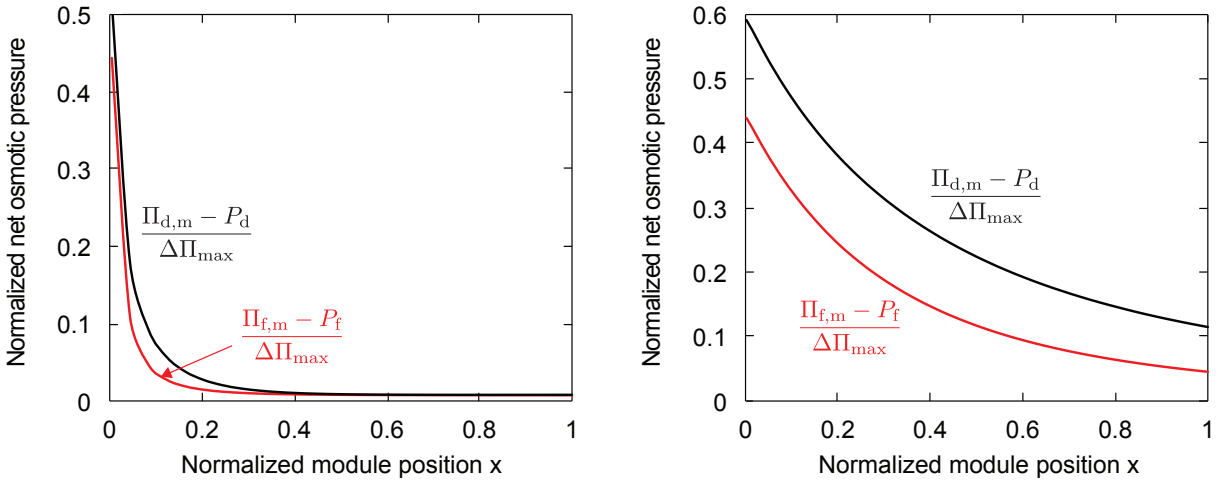

(a) $J_{\min} = 0$ L/m^2-hr (b) $J_{\min} = 10$ L/m^2-hr

Figure 17: Normalized net osmotic pressure as a function of normalized module position. The osmotic driving force is normalized by the maximum osmotic pressure difference (i.e., $\Delta\Pi_{max} = \Pi_{d,in} - \Pi_{f,in}$). The module position is normalized by the length of the module. The difference between the two lines is the osmotic driving force.

Figure 17 visualizes the osmotic driving force with $J_{\min} = 0$ L/m^2-hr and $J_{\min} = 10$ L/m^2-hr. The osmotic driving force is the difference between the net osmotic pressures which are defined as $\Pi_{net} = \Pi - P$ for each stream. The osmotic pressure at the membrane surface is used to correctly quantify the driving force. When $J_{\min}$ is 10 L/m^2-hr, the osmotic driving force is relatively uniformly distributed, and further increase in the system size only perturbs this distribution. Therefore, the marginal return of increasing the system size is small. As a result, the combined PRO-desalination system does not produce net energy even with $J_{\min} = 0$ L/m^2-hr unlike the reversible blackbox mixer in Fig. 8. The PRO system is an irreversible system, and it has a large membrane area, which results in zero driving force only at one end of the PRO system. However, zero driving force at one location does not imply that the system is reversible because osmosis occurs through a finite osmotic pressure difference throughout the system, which generates entropy. A completely reversible system is one in which the driving force is everywhere zero. The driving force in this case is the difference between the net osmotic pressures (i.e., $\Pi_{net,d} - \Pi_{net,f} = (\Pi_{d,m} - P_d) - (\Pi_{f,m} - P_f)$). The hydraulic pressure on both sides is relatively constant assuming that viscous losses are small compared to the osmotic pressure, which varies along the length of the system due to variation in the salinities of the streams. In order to cancel the driving force everywhere in the system, the hydraulic pressure difference

has to continuously equal the osmotic pressure difference. The PRO system that was modeled raises the pressure of the draw solution only once before it enters the module (hence the single-pressure operation), which is why the driving force is finite throughout the system except at one end of the module (for the case of $J_{\min} = 0$ L/m^2-hr) as shown in Fig. 17a.

Because each data point in Fig. 16 is a result of optimization, changing the operating conditions will not result in a decrease in the net energy input. This suggests that the single-pressure operation, which is by far the most widely studied configuration, does not have much potential to save significant energy from a desalination plant (limited to about 0.42 kWh/m^3). In PRO literature, not many researchers have considered module-scale operation. Most of the studies use coupon-scale system where the osmotic driving force is virtually uniform inside the system [22, 23, 51]. Few researchers studied the variation of the osmotic driving force of a module-scale system. For example, Banchik et al. developed the concept of mass transfer unit (MTU) to properly represent the difference between coupon and module-scale systems [29, 54]. This is why the limitation of single stage operation resulting from its poor distribution of driving force has not been stressed. Different configurations such as multistaging or batch operation can distribute the osmotic driving force more effectively over the PRO module. Therefore, these configurations may have potential to increase the energy saving.

4. Conclusions

Two distinctly different ways of managing desalination brine are analyzed from an energetic perspective: zero-discharge desalination (ZDD) with salt production and electricity generation utilizing the exergy of the brine. Thermodynamic minimum energy required for ZDD process was calculated. In particular, energy required for brine concentration stage was compared to that required for crystallization to identify which stage has greater potential for improvement. State-of-the-art technologies for brine concentration and crystallization were analyzed using the concept of Second Law efficiency.

For energy generation, we applied the First and Second Laws of thermodynamics to reversible, blackbox systems. Then the same analysis was applied to a practical salinity-gradient system, PRO. A detailed numerical model for the PRO was used along with a nonlinear optimization to determine the optimal operating conditions. The energy saving by adding a PRO unit to a desalination system was quantified.

Our primary results are as follows:

Blackbox (reversible) systems

- The least work required for concentrating a feed until saturation and then for completely crystallizing saturated brine was obtained for feed salinities 0-260 g/kg.

- For feed water salinities near that of seawater, the magnitudes of the least work for brine concentration and crystallization are similar even though the volume reduction achieved in the crystallization step is around an order of magnitude smaller than that achieved in the brine concentration step.
- Absolute energy required for brine concentration until saturation and that required for complete crystallization thereafter, are comparable in order of magnitude for feed salinities up to 120 g/kg.
- Reversible systems can generate more energy from mixing the desalination brine with an independent stream at low salinity and high flow rate, than the energy required for desalination.

Process-specific implementations

- State-of-the-art crystallizers were found to be more efficient than state-of-the-art brine concentrators. While a 6-effect thermal evaporator had a Second Law efficiency of 24.4%, a conventional single-effect MVC brine concentrator had an efficiency of only 8.5% while a two-effect MVC brine concentrator was marginally better with an efficiency of 11.6%.
- Research efforts around zero-discharge desalination should focus on improving brine concentration rather than crystallization as the former has a larger room for improvement.
- Energy savings achieved by adding a PRO unit (with single-pressure operation) to a desalination system are not significant.
- A PRO system using an independent dilute stream and coupled with a desalination system cannot produce net positive energy, in contrast to the reversible blackbox mixer because of inherent irreversibilities associated with a finite osmotic driving force.
- The single-pressure operation of PRO has an ineffectively distributed osmotic driving force over the module. Different configurations such as multistaging or batch operation may have potential because they distribute the osmotic pressure in a more effective way.

With a proper understanding of the energetic aspects of zero-discharge brine management and salinity-gradient power production, the natural next step is an economic analysis because economic viability will ultimately determine the adoption of any technology. In addition to the traditional costs associated with these technologies, location-dependent factors, such as the prices of energy, salt, and water, should be taken into account. Low energy prices, and high prices of salt and water will push for the adoption of ZDD, and the opposite will favor the adoption of salinity-gradient power generation.

5. Acknowledgements

The authors would like to thank Kuwait Foundation for the Advancement Sciences (KFAS) for their financial support through Project No. P31475EC01.

References

[1] IDA Desalination Yearbook 2015-2016, Media Analytics Ltd., 2015.

[2] IDA Desalination Yearbook 2014-2015, Media Analytics Ltd., 2014.

[3] IDA Desalination Yearbook 2013-2014, Media Analytics Ltd., 2013.

[4] IDA Desalination Yearbook 2012-2013, Media Analytics Ltd., 2012.

[5] IDA Desalination Yearbook 2011-2012, Media Analytics Ltd., 2011.

[6] IDA Desalination Yearbook 2010-2011, Media Analytics Ltd., 2010.

[7] M. Wilf, L. Awerbuch, C. Bartels, M. Mickley, G. PearcNikolay, Voutchkov, The Guidebook to Membrane Desalination Technology : Reverse Osmosis, Nanofiltration and Hybrid Systems Process, Design, Applications and Economics, Balaban Publishers, 2011.

[8] H. Strathmann, Electrodialysis, a mature technology with a multitude of new applications, Desalination 264 (3) (2010) 268–288. doi:10.1016/j.desal.2010.04.069.
URL http://dx.doi.org/10.1016/j.desal.2010.04.069

[9] Y. Kobuchi, Y. Terada, Y. Tani, The First Salt Plant in the Middle East Using Electrodialysis and Ion Exchange Membranes, Sixth International Symposium on Salt ll (1983) 541–555.

[10] T. A. Davis, Zero discharge seawater desalination: Integrating the production of freshwater, salt, magnesium, and bromine, Tech. Rep. 111, Bureau of Reclamation, US Department of Interior (2006).

[11] V. M. Sedivy, Environmental Balance of Salt Production speaks in favour of Solar Saltworks, Global NEST Journal 11 (1) (2009) 41–48.

[12] B. Ericsson, B. Hallmans, Treatment of saline wastewater for zero discharge at the Debiensko coal mines in Poland, Desalination 105 (1-2) (1996) 115–123. doi:10.1016/0011-9164(96)00065-3.

[13] IDE Technologies, IDE-Tech MVC Brochure (2016).
URL http://www.ide-tech.com/wp-content/uploads/2013/09/Mechanical-Vapour-Compression-MVC-Brochure.pdf

[14] A. Ravizky, N. Nadav, Salt production by the evaporation of SWRO brine in Eilat: a success story, Desalination 205 (1-3) (2007) 374–379. doi:10.1016/j.desal.2006.03.559.

[15] R. K. McGovern, S. M. Zubair, J. H. Lienhard V, The cost effectiveness of electrodialysis for diverse salinity applications, Desalination 348 (2014) 57–65. doi:10.1016/j.desal.2014.06.010.
URL http://www.sciencedirect.com/science/article/pii/S0011916414003312

[16] M. Ahmed, A. Arakel, D. Hoey, M. R. Thumarukudy, M. F. a. Goosen, M. Al-Haddabi, A. Al-Belushi, Feasibility of salt production from inland RO desalination plant reject brine: A case study, Desalination 158 (1-3) (2003) 109–117. doi:10.1016/S0011-9164(03)00441-7.

[17] C. M. Tun, A. G. Fane, J. T. Matheickal, R. Sheikholeslami, Membrane distillation crystallization of concentrated salts—flux and crystal formation, Journal of Membrane Science 257 (1–2) (2005) 144 – 155, membrane Contactors. doi:10.1016/j.memsci.2004.09.051.
URL http://www.sciencedirect.com/science/article/pii/S0376738804008361

[18] R. Creusen, J. van Medevoort, M. Roelands, A. van Renesse van Duivenbode, J. H. Hanemaaijer, R. van Leerdam, Integrated membrane distillation–crystallization: Process design and cost estimations for seawater treatment and fluxes of single salt solutions, Desalination 323 (2013) 8 – 16, membrane Distillation and related Membrane Systems. doi:10.1016/j.desal.2013.02.013.
URL http://www.sciencedirect.com/science/article/pii/S0011916413000763

[19] F. Edwie, T.-S. Chung, Development of simultaneous membrane distillation–crystallization (SMDC) technology for treatment of saturated brine, Chemical Engineering Science 98 (2013) 160 – 172. doi:10.1016/j.ces.2013.05.008.
URL http://www.sciencedirect.com/science/article/pii/S0009250913003291

[20] G. Chen, Y. Lu, W. B. Krantz, R. Wang, A. G. Fane, Optimization of operating conditions for a continuous membrane distillation crystallization process with zero salty water discharge, Journal of Membrane Science 450 (2014) 1 – 11. doi:10.1016/j.memsci.2013.08.034.
URL http://www.sciencedirect.com/science/article/pii/S0376738813007011

[21] S. Meng, Y. Ye, J. Mansouri, V. Chen, Crystallization behavior of salts during membrane distillation with hydrophobic and superhydrophobic capillary membranes, Journal of Membrane Science 473 (2015) 165 – 176. doi:10.1016/j.memsci.2014.09.024.
URL http://www.sciencedirect.com/science/article/pii/S0376738814007170

[22] G. Z. Ramon, B. J. Feinberg, E. M. V. Hoek, Membrane-based production of salinity-gradient power, Energy Environ. Sci. 4 (2011) 4423–4434. doi:10.1039/C1EE01913A.
URL http://dx.doi.org/10.1039/C1EE01913A

[23] J. W. Post, J. Veerman, H. V. Hamelers, G. J. Euverink, S. J. Metz, K. Nymeijer, C. J. Buisman, Salinity-gradient power: Evaluation of pressure-retarded osmosis and reverse electrodialysis, Journal of Membrane Science 288 (1–2) (2007) 218 – 230. doi:http://dx.doi.org/10.1016/j.memsci.2006.11.018.
URL http://www.sciencedirect.com/science/article/pii/S0376738806007575

[24] A. M. Weiner, R. K. McGovern, J. H. Lienhard V, A new reverse electrodialysis design strategy which significantly reduces the levelized cost of electricity, Journal of Membrane Science 493 (2015) 605 – 614. doi:10.1016/j.memsci.2015.05.058.
URL http://www.sciencedirect.com/science/article/pii/S0376738815004962

[25] A. M. Weiner, R. K. McGovern, J. H. Lienhard V, Increasing the power density and reducing the levelized cost of electricity of a reverse electrodialysis stack through blending, Desalination 369 (2015) 140 – 148. doi:10.1016/j.desal.2015.04.031.
URL http://www.sciencedirect.com/science/article/pii/S0011916415002842

[26] X. Song, Z. Liu, D. D. Sun, Energy recovery from concentrated seawater brine by thin-film nanofiber composite pressure retarded osmosis membranes with high power density, Energy Environ. Sci. 6 (2013) 1199–1210. doi:10.1039/C3EE23349A.
URL http://dx.doi.org/10.1039/C3EE23349A

[27] K. Saito, M. Irie, S. Zaitsu, H. Sakai, H. Hayashi, A. Tanioka, Power generation with salinity gradient by pressure retarded osmosis using concentrated brine from swro system and treated sewage as pure water, Desalination and Water Treatment 41 (1-3) (2012) 114–121. doi:10.1080/19443994.2012.664696.
URL http://dx.doi.org/10.1080/19443994.2012.664696

[28] J. L. Prante, J. A. Ruskowitz, A. E. Childress, A. Achilli, RO-PRO desalination: An integrated low-energy approach to seawater desalination, Applied Energy 120 (2014) 104 – 114. doi:http://dx.doi.org/10.1016/j.apenergy.2014.01.013.
URL http://www.sciencedirect.com/science/article/pii/S0306261914000324

[29] L. D. Banchik, M. H. Sharqawy, J. H. Lienhard V, Limits of power production due to finite membrane area in pressure retarded osmosis, Journal of Membrane Science 468 (2014) 81 – 89. doi:10.1016/j.memsci.2014.05.021.
URL http://www.sciencedirect.com/science/article/pii/S037673881400386X

[30] G. P. Thiel, E. W. Tow, L. D. Banchik, H. W. Chung, J. H. Lienhard V, Energy consumption in

desalinating produced water from shale oil and gas extraction, Desalination 366 (2015) 94 – 112. doi:http://dx.doi.org/10.1016/j.desal.2014.12.038.
URL http://www.sciencedirect.com/science/article/pii/S0011916414006857

[31] K. H. Mistry, J. H. Lienhard V, Effect of Nonideal Solution Behavior on Desalination of a Sodium Chloride Solution and Comparison to Seawater, Journal of Energy Resources Technology 135 (4) (2013) 042003. doi:10.1115/1.4024544.
URL http://energyresources.asmedigitalcollection.asme.org/article.aspx?doi=10.1115/1.4024544

[32] F. Van der Ham, Eutectic Freeze Crystallization, Ph.D. thesis, Technical University Delft (1999). arXiv:arXiv:1011.1669v3, doi:10.1017/CBO9781107415324.004.

[33] G. P. Thiel, J. H. Lienhard V, Treating produced water from hydraulic fracturing: Composition effects on scale formation and desalination system selection, Desalination 346 (2014) 54 – 69. doi:10.1016/j.desal.2014.05.001.
URL http://www.sciencedirect.com/science/article/pii/S0011916414002574

[34] K. S. Pitzer, Thermodynamics of electrolytes. I. Theoretical basis and general equations, The Journal of Physical Chemistry 77 (2) (1973) 268–277. doi:10.1021/j100621a026.
URL http://dx.doi.org/10.1021/j100621a026

[35] K. S. Pitzer, J. J. Kim, Thermodynamics of electrolytes. IV. Activity and osmotic coefficients for mixed electrolytes, Journal of the American Chemical Society 96 (18) (1974) 5701–5707. doi:10.1021/ja00825a004.
URL http://dx.doi.org/10.1021/ja00825a004

[36] D. J. Bradley, K. S. Pitzer, Thermodynamics of Electrolytes. 12. Dielectric Properties of Water and Debye-Hückel Parameters to 350° C and 1 kbar, The Journal of Physical Chemistry 83 (12) (1979) 1599–1603.

[37] K. S. Pitzer, J. C. Peiper, R. H. Busey, Thermodynamic Properties of Aqueous Sodium Chloride Solutions, Journal of Physical and Chemical Reference Data 13 (1) (1984) 1–102. doi:10.1063/1.555709.
URL http://scitation.aip.org/content/aip/journal/jpcrd/13/1/10.1063/1.555709

[38] K. S. Pitzer, A thermodynamic model for aqueous solutions of liquid-like density, Reviews in Mineralogy and Geochemistry 17 (1987) 97–142.

[39] J. F. Zemaitis, D. M. Clark, M. Rafal, N. C. Scrivner, Handbook of Aqueous Electrolyte Thermodynamics, Wiley-AIChE, 1986.

[40] K. H. Mistry, R. K. McGovern, G. P. Thiel, E. K. Summers, S. M. Zubair, J. H. Lienhard V, Entropy generation analysis of desalination technologies, Entropy 13 (10) (2011) 1829–1864. doi:10.3390/e13101829.
URL http://www.mdpi.com/1099-4300/13/10/1829

[41] S. A. Klein, G. F. Nellis, Thermodynamics, Cambridge University Press, 2011.

[42] K. G. Nayar, M. H. Sharqawy, L. D. Banchik, J. H. Lienhard V, Thermophysical properties of seawater: A review and new correlations that include pressure dependence, Desalination 387 (2016) 1–24. doi:10.1016/j.desal.2016.02.024.
URL http://web.mit.edu/seawater/

[43] J. Swaminathan, K. G. Nayar, J. H. Lienhard V, Mechanical vapor compression—membrane distillation hybrids for reduced specific energy consumption, Desalination and Water Treatment 57 (55) (2016) 26507–26517. doi:10.1080/19443994.2016.1168579.
URL http://www.tandfonline.com/doi/full/10.1080/19443994.2016.1168579

[44] H. T. El-Dessouky, H. M. Ettouney, Fundamentals of Salt Water Desalination, Elsevier, Amsterdam, 2002.

[45] A. Morris, The use of titanium tubes in msf desalination plants, Desalination 31 (1) (1979) 387. doi:10.1016/S0011-9164(00)88539-2.
URL http://www.sciencedirect.com/science/article/pii/S0011916400885392

[46] J. Green, B. Gamson, W. Westerbaan, Experience with desalination plants containing titanium heat exchange tubing, Desalination 22 (1) (1977) 359 – 368. doi:10.1016/S0011-9164(00)88391-5.
URL http://www.sciencedirect.com/science/article/pii/S0011916400883915

[47] S. A. Klein, Engineering Equation Solver.

[48] H. W. Chung, L. D. Banchik, J. Swaminathan, J. H. Lienhard V, On the present and future economic viability of stand-alone pressure-retarded osmosis, Desalination (under review).

[49] N. Y. Yip, A. Tiraferri, W. A. Phillip, J. D. Schiffman, L. A. Hoover, Y. C. Kim, M. Elimelech, Thin-film composite pressure retarded osmosis membranes for sustainable power generation from salinity

gradients, Environmental Science & Technology 45 (10) (2011) 4360–4369. doi:10.1021/es104325z.
URL http://dx.doi.org/10.1021/es104325z

[50] G. Schock, A. Miquel, Mass transfer and pressure loss in spiral wound modules, Desalination 64 (1987) 339 – 352. doi:10.1016/0011-9164(87)90107-X.
URL http://www.sciencedirect.com/science/article/pii/001191648790107X

[51] A. Achilli, T. Y. Cath, A. E. Childress, Power generation with pressure retarded osmosis: An experimental and theoretical investigation, Journal of Membrane Science 343 (1–2) (2009) 42 – 52. doi:10.1016/j.memsci.2009.07.006.
URL http://www.sciencedirect.com/science/article/pii/S0376738809005134

[52] C. Fritzmann, J. Löwenberg, T. Wintgens, T. Melin, State-of-the-art of reverse osmosis desalination, Desalination 216 (1–3) (2007) 1 – 76. doi:http://dx.doi.org/10.1016/j.desal.2006.12.009.
URL http://www.sciencedirect.com/science/article/pii/S0011916407004250

[53] E. W. Tow, R. K. McGovern, J. H. Lienhard V, Raising forward osmosis brine concentration efficiency through flow rate optimization, Desalination 366 (2015) 71 – 79. doi:10.1016/j.desal.2014.10.034.
URL http://www.sciencedirect.com/science/article/pii/S0011916414005578

[54] M. H. Sharqawy, L. D. Banchik, J. H. Lienhard V, Effectiveness–mass transfer units (ε–MTU) model of an ideal pressure retarded osmosis membrane mass exchanger, Journal of Membrane Science 445 (2013) 211 – 219. doi:10.1016/j.memsci.2013.06.027.
URL http://www.sciencedirect.com/science/article/pii/S0376738813005206